Calibration and Rectification for Reflection Stereo

Masao Shimizu and Masatoshi Okutomi
Tokyo Institute of Technology, Japan

Abstract

This paper presents a calibration and rectification method for single-camera range estimation using a single complex image with a transparent plate or a double-sided half-mirror plate, which are collectively called a reflection stereo. The range to an object is obtainable by finding the correspondence on a constraint line in the complex image, which consists of a surface and a rear-surface reflected image in the transparent plate, or also includes a transmitted and internal reflected image through a double-sided half-mirror plate. The range estimation requires extrinsic parameters of the reflection stereo that include the shape and position of the plate and its refraction index. The proposed method assumes that the plate is non-parallel but planar for a local region around the point of interest in the complex image. The method estimates the extrinsic parameters from a set of displacements in the complex images. Experiments using real images demonstrate the effectiveness of the proposed calibration and rectification method along with fine range estimation results.

1. Introduction

A complex image is visible in a reflection on a transparent plate if subjected to careful observation. The complex image consists of the surface and rear-surface reflection of the plate; the displacement between the reflections in the image depends on the orientation of the plate and the object distance.

The complex image is also observed through a double-sided half-mirror plate, which has two half-mirrors on both sides of the plate. The transmitted light on the incident side half-mirror of the plate is partly transmitted at the exit-side half-mirror and the rest is reflected. The transmitted light (the direct image) reaches the camera, but some reflected light reflects again at the incident-side half-mirror and subsequently reaches the camera through the exit-side half-mirror (the internal reflection image). These light paths produce a complex image with displacement and different intensities between reflections.

Reflection stereo is a type of single-camera stereo rig with a transparent or a double-sided half-mirror plate to generate the complex image. The stereo rigs are respectively called reflection-type [12] and transmission-type [13]. The reflection stereo can estimate the object range using a single camera, without any moving mechanisms.

Stereo vision is an extremely active research area; object range and shape estimation methods using a single camera have been studied widely. Single-camera methods can be categorized as multi-view [4],[7], multi-image [3],[10], and multi-exposure [5],[11] methods. The reflection stereo belongs to the last category.

This paper presents a calibration and image rectification method for the reflection stereo. The displacement in the complex image depends not only on the object range, but also on the normal vectors of the plate surfaces, plate thickness, relative refraction index, and the plate position. The proposed method assumes that the plate is non-parallel and piecewise planar. The proposed calibration method estimates these parameters of the transparent plate using multiple planar targets with random textures at known distances. Through calibration, an accurate constraint is obtainable for the effective corresponding search in the complex image.

The calibration method can also be considered as a shape and refraction index estimation method for a transparent object. Some methods have been proposed for this end, for example detection of the optical flow of the background through a transparent object [9], and tracing the structured ray through a transparent object [8]. Every existing method uses direct transmitted rays, but the reflection stereo makes use of the internally reflected ray in the transparent object.

The feasibility of reconstructing the shape and refraction index of an object has been investigated [6]. The investigation assumes that a ray reflects or refracts perfectly (not both simultaneously) on an object surface. Therefore, only a unique light path exists from a reference point to a view point. The reflection stereo uses multiple light paths from an object to a camera to form the complex image.

This paper is organized as follows. Section 2 de-

978-1-4244-2243-2/08/$25.00 ©2008 IEEE

scribes range estimation by reflection stereo with a perfectly parallel planar transparent and double-sided half-mirror plate. Section 3 extends to the case with a non-parallel planar plate and shows the parameters to be estimated. Section 4 presents a method to estimate the parameters using multiple targets and corresponding displacements in the complex images. A rectification method for the complex image is presented in Section 5. Experimental results are described in Section 6. This paper concludes with remarks in Section 7.

2. Reflection Stereo

2.1. Reflection-Type Configuration

Figure 1 shows two light paths from an object to the optical center. A transparent plate reflects and transmits the incident light on its surface. The transmitted light is then reflected on the rear surface and is transmitted again to the air through the surface. These two light paths have an angle disparity θ_s, which depends on the relative refractive index n of the plate, the plate thickness d, the incident angle θ_i, and the object distance D_o.

The fundamental relation between the angle disparity θ_s and the distance D_o are explainable as the reflection and refraction of light in a plane including the object, the optical center, and the normal vector of the plate. A two-dimensional (2D) ξ-υ coordinate system is set with its origin at the reflecting point on the surface. The following equation can be derived by projecting the object position $(-D_o \sin\theta_i, D_o \cos\theta_i)$ and the optical center position $(D_c \sin\theta_i, D_c \cos\theta_i)$ to ξ-axis.

$$D_o + D_c = d\frac{\sin\left(2\left(\theta_i - \theta_s\right)\right)}{\sin\theta_s\sqrt{n^2 - \sin^2\left(\theta_i - \theta_s\right)}} \qquad (1)$$

The angle disparity θ_s is obtainable by finding the displacement in the complex image. Then the object distance D_o is derived from Eq. (1). The displacement has a constraint which describes a correspondent position in the rear-surface image moving along a constraint line according to the image position [12]. The

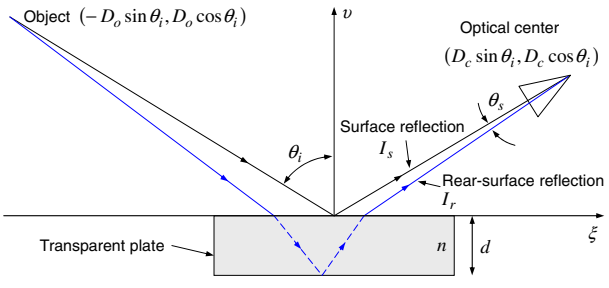

Figure 1. Geometry of the reflection-type configuration.

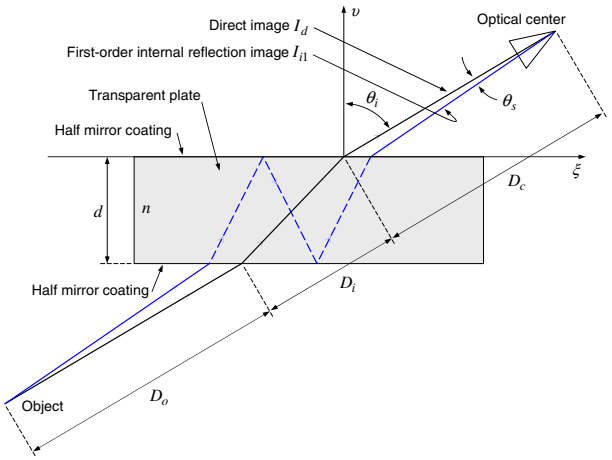

Figure 2. Geometry of the transmission-type configuration.

constraint reduces the search to 1D, just as stereo vision with the epipolar constraint. The angle disparity takes the minimum value $\theta_s = 0$ when $D_o = \infty$ if the plate is manufactured perfectly as a parallel planar plate.

2.2. Transmission-Type Configuration

Figure 2 presents the direct image I_d and the internal reflection image I_i from an object to the optical center. These two light paths also have an angle disparity θ_s, which depends on the relative refractive index n of the plate, the plate thickness d, the incident angle θ_i, and the object distance D_o. A 2D ξ-υ coordinate system is set with its origin at the intersection of the direct light path and the exit-side half-mirror. The following equation can be derived by projecting the object distance $D_o + D_i + D_c$ along the direct image and the internal reflected image light paths to ξ-axis.

$$D_o + D_i + D_c = d\frac{\dfrac{3\sin(\theta_i - \theta_s)}{\sqrt{n^2 - \sin^2(\theta_i - \theta_s)}} - \dfrac{\sin\theta_i}{\sqrt{n^2 - \sin^2\theta_i}}}{\dfrac{\sin\theta_s}{\cos(\theta_i - \theta_s)}} + d\left(\cos\theta_i + \frac{\sin^2\theta_i}{\sqrt{n^2 - \sin^2\theta_i}}\right) \qquad (2)$$

2.3. Object Range

Reflection stereo with a parallel planar plate requires not only a lens focal length in CCD pixel units of f/δ as a parameter, but also the following parameters, which are equivalent to extrinsic parameters in stereo vision.

- surface normal $\mathbf{n}_m$ of the plate,
- surface position Dco from the optical center along the lens optical axis,

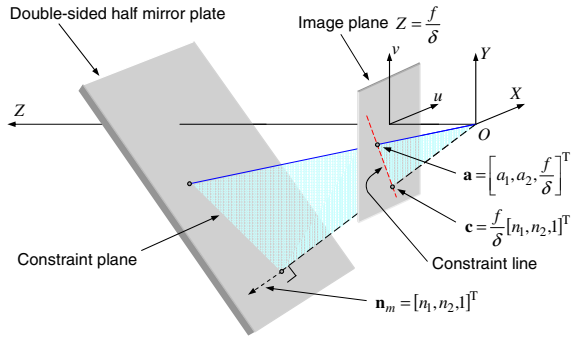

Figure 3. Constraint line on the image plane.

- plate thickness d, and
- relative refraction index n.

With these five extrinsic parameters, the object range is obtainable using Eq. (1) or Eq. (2) with a displacement in a complex image.

Figure 3 depicts the camera coordinate system, with its origin at the optical center. We assume that a correspondence position for the image position $A(\mathbf{a}) = [a_1, a_2, f/\delta]^\top$ is located at a relative distance Δ [pixel] from A along the constraint line. The angle disparity θ_s is obtainable as

$$\theta_s = \cos^{-1}\left(\frac{\mathbf{a}\cdot(\mathbf{a}+\mathbf{e}(\mathbf{a})\Delta)}{\|\mathbf{a}\|\|\mathbf{a}+\mathbf{e}(\mathbf{a})\Delta\|}\right), \tag{3}$$

where $\mathbf{e}(\mathbf{a}) = \dfrac{\mathbf{c}-\mathbf{a}}{\|\mathbf{c}-\mathbf{a}\|}$ denotes a unit vector of the constraint line at the position $\mathbf{a}$ to $\mathbf{c} = f/\delta[n_1, n_2, 1]^\top$.

The incident angle of the position $\mathbf{a}$ to the plate is obtainable as the following.

$$\theta_i = \cos^{-1}\left(\frac{\mathbf{a}\cdot\mathbf{n}_m}{\|\mathbf{a}\|\|\mathbf{n}_m\|}\right) \tag{4}$$

The complex image can be considered as a signal that consists of two identical signals with a shift along the constraint line. The autocorrelation function of the signal generally has three peaks at the origin, and at the plus and minus shifts. This allows estimation of the displacement in the complex image without any feature points or edges if the object has some texture. In the transmission-type configuration, the two images in a complex image have different intensities. Correspondence indices, including the peak curvature, help to ascertain the displacement [13].

3. Non-Parallel and Non-Planar Plate

3.1. Piecewise Planar Model

Any transparent plate or half-mirror plate has imperceptible surface shape faultiness. The plates are non-parallel and non-planar.

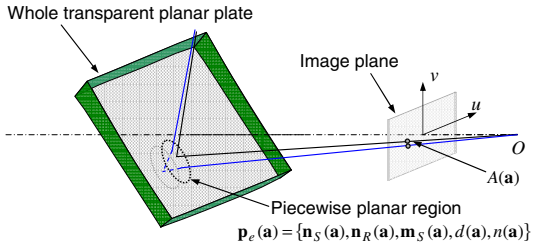

Figure 4. Extrinsic parameters for a non-parallel and piecewise planar model.

The proposed method assumes that the plate is non-parallel but piecewise planar, as illustrated in Fig. 4. In other words, the method assumes that the extrinsic parameters are constant in a small region to form a complex image around an interest position. The extended extrinsic parameters include the normal vectors for each side of the plate, as follows.

- surface normals $\mathbf{n}_R$ and $\mathbf{n}_S$ of the plate,
- surface position Dco from the optical center along the lens optical axis,
- plate thickness d, and
- relative refraction index n.

These seven extrinsic parameters $\mathbf{p}_e(\mathbf{a}) = \{\mathbf{n}_R(\mathbf{a}), \mathbf{n}_S(\mathbf{a}), Dco(\mathbf{a}), d(\mathbf{a}), n(\mathbf{a})\}$ are positionally variant.

In our experiments, the complex image is observed from about a 45×40 [mm^2] area in a plate. The small region that is assumed to have a constant extrinsic parameters is about 1.4×2.5 [mm^2], with the situation that the image size is 640×480 [pixel], the small region size is 20×20 [pixel], and the displacement in the complex image is 20 [pixel]. The first-order shape approximation for such a small area is sufficient to obtain accurate constraint and range estimation.

3.2. Object Range

The object range is obtainable with the displacement in the complex image and the extrinsic parameters $\mathbf{p}_e(\mathbf{a})$ using the ray tracing algorithm.

3.2.1 Reflection-Type Configuration

Figure 5(a) shows that an object in a surface reflection image at an image position $A(\mathbf{a}) = [u_a, v_a, f/\delta]^\top$ exists in the following line $\mathbf{L}_S$ with parameter t_S:

$$\begin{aligned} \mathbf{L}_S(t_S) &= \mathbf{q}_S + \mathbf{v}_S t_S \\ \mathbf{q}_S &= \mathbf{q}(\mathbf{o}, \mathbf{a}, \mathbf{m}_S, \hat{\mathbf{n}}_S) \\ \mathbf{v}_S &= \mathbf{r}(\mathbf{a}, \hat{\mathbf{n}}_S) \end{aligned} \tag{5}$$

where $M_S(\mathbf{m}_S)$ and $\hat{\mathbf{n}}_S$ respectively denote a position and the unit normal vector of the plate surface. Point $O(\mathbf{o})$ represents the origin.

Similarly, a detected relative displacement $\mathbf{d} = \mathbf{d}_p^*(\mathbf{a}) + \mathbf{e}^*(\mathbf{a})\Delta$ of a rear-surface reflection image from a surface reflection image position $\mathbf{a}$ shows that the object in the rear-surface image exists in the following line $\mathbf{L}_R$ with parameter t_R.

$$\begin{aligned} \mathbf{L}_R(t_R) &= \mathbf{q}_R + \mathbf{v}_R t_R \\ \mathbf{q}_R &= \mathbf{q}(\mathbf{q}_1, \mathbf{v}_1, \mathbf{m}_S, \hat{\mathbf{n}}_S) \\ \mathbf{v}_R &= \mathbf{t}(\mathbf{v}_1, -\hat{\mathbf{n}}_S, 1/n) \\ \mathbf{q}_1 &= \mathbf{q}(\mathbf{q}_0, \mathbf{v}_0, \mathbf{m}_R, \hat{\mathbf{n}}_R) \\ \mathbf{v}_1 &= \mathbf{r}(\mathbf{v}_0, \hat{\mathbf{n}}_R) \\ \mathbf{q}_0 &= \mathbf{q}(\mathbf{o}, \mathbf{a}+\mathbf{d}, \mathbf{m}_S, \hat{\mathbf{n}}_S) \\ \mathbf{v}_0 &= \mathbf{t}(\mathbf{a}+\mathbf{d}, \hat{\mathbf{n}}_S, n) \end{aligned} \tag{6}$$

Therein, $M_R(\mathbf{m}_R)$ and $\hat{\mathbf{n}}_R$ respectively denote a position and the unit normal vector of the rear surface of the plate, as shown in Fig. 5(b). In addition, $\mathbf{d}_p^*(\mathbf{a})$ and $\mathbf{e}^*(\mathbf{a})$ denote the displacement of the rear-surface reflection image for an object at infinite distance and a unit vector of the constraint line at the image position $\mathbf{a}$ (refer to **3.3.**).

The intersection position of lines $\mathbf{L}_S$ and $\mathbf{L}_R$ represents the 3D position $P_O(\hat{\mathbf{p}}_O)$ of the object. In real situations, the object position $P_O(\hat{\mathbf{p}}_O)$ is determined using the following equation, which minimizes the distance between the two lines.

$$\hat{\mathbf{p}}_O = \frac{1}{2}\left[(\mathbf{q}_S + \mathbf{v}_S t_S) + (\mathbf{q}_R + \mathbf{v}_R t_R)\right] \tag{7}$$

$$\begin{bmatrix} t_S \\ t_R \end{bmatrix} = \begin{bmatrix} \mathbf{q}_S \cdot \mathbf{v}_S & -\mathbf{q}_S \cdot \mathbf{v}_R \\ \mathbf{q}_R \cdot \mathbf{v}_S & -\mathbf{q}_R \cdot \mathbf{v}_R \end{bmatrix}^{-1} \begin{bmatrix} \mathbf{q}_S \cdot \mathbf{q}_R - \|\mathbf{q}_S\|^2 \\ \|\mathbf{q}_R\|^2 - \mathbf{q}_S \cdot \mathbf{q}_R \end{bmatrix}$$

3.2.2 Transmission-Type Configuration

Figure 6(a) shows that an object in a direct image at an image position $A(\mathbf{a})$ exists in the following line $\mathbf{L}_D$

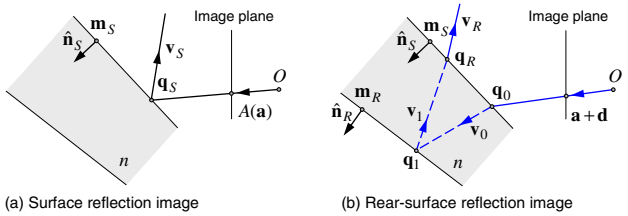

Figure 5. Surface and rear-surface reflection images.

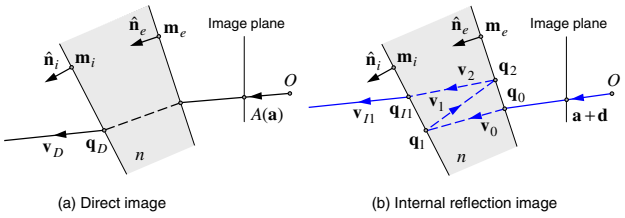

Figure 6. Direct and internal reflection images.

with parameter t_D:

$$\begin{aligned} \mathbf{L}_D(t_D) &= \mathbf{q}_D + \mathbf{v}_D t_D \\ \mathbf{q}_D &= \mathbf{q}(\mathbf{q}(\mathbf{o}, \mathbf{a}, \mathbf{m}_e, \hat{\mathbf{n}}_e), \mathbf{t}(\mathbf{a}, \hat{\mathbf{n}}_e, n), \mathbf{m}, \hat{\mathbf{n}}_i) \\ \mathbf{v}_D &= \mathbf{t}(\mathbf{t}(\mathbf{a}, \hat{\mathbf{n}}_e, n), \hat{\mathbf{n}}_i, 1/n), \end{aligned} \tag{8}$$

where $M_i(\mathbf{m}_i)$ and $M_e(\mathbf{m}_e)$ respectively represent positions on the incident and exit-side half-mirror surfaces; in addition, $\hat{\mathbf{n}}_i$ and $\hat{\mathbf{n}}_e$ respectively denote the unit normal vector of incident and exit-side half-mirror surfaces.

Similarly, the corresponding object in an internal reflection image at a relative displacement $\mathbf{d} = \mathbf{d}_p^*(\mathbf{a}) + \mathbf{e}^*(\mathbf{a})\Delta$ from a direct image position $\mathbf{a}$ exists in the following line $\mathbf{L}_{I1}$ with parameter t_{I1}, as shown in Fig. 6(b).

$$\begin{aligned} \mathbf{L}_{I1}(t_{I1}) &= \mathbf{q}_{I1} + \mathbf{v}_{I1} t_{I1} \\ \mathbf{q}_{I1} &= \mathbf{q}(\mathbf{q}_2, \mathbf{v}_2, \mathbf{m}_i, \hat{\mathbf{n}}_i) \\ \mathbf{v}_{I1} &= \mathbf{t}(\mathbf{v}_2, \hat{\mathbf{n}}_i, 1/n) \\ \mathbf{q}_2 &= \mathbf{q}(\mathbf{q}_1, \mathbf{v}_1, \mathbf{m}_e, \hat{\mathbf{n}}_e) \\ \mathbf{v}_2 &= \mathbf{r}(\mathbf{v}_1, -\hat{\mathbf{n}}_e) \\ \mathbf{q}_1 &= \mathbf{q}(\mathbf{q}_0, \mathbf{v}_0, \mathbf{m}_i, \hat{\mathbf{n}}_i) \\ \mathbf{v}_1 &= \mathbf{r}(\mathbf{v}_0, \hat{\mathbf{n}}_i) \\ \mathbf{q}_0 &= \mathbf{q}(\mathbf{o}, \mathbf{a}+\mathbf{d}, \mathbf{m}_e, \hat{\mathbf{n}}_e) \\ \mathbf{v}_0 &= \mathbf{t}(\mathbf{a}+\mathbf{d}, \hat{\mathbf{n}}_e, n) \end{aligned} \tag{9}$$

The intersection position of lines $\mathbf{L}_D$ and $\mathbf{L}_{I1}$ represents the 3D position $\hat{\mathbf{p}}_O$ of the object.

$$\hat{\mathbf{p}}_O = \frac{1}{2}\left[(\mathbf{q}_D + \mathbf{v}_D t_D) + (\mathbf{q}_{I1} + \mathbf{v}_{I1} t_{I1})\right] \tag{10}$$

$$\begin{bmatrix} t_D \\ t_{I1} \end{bmatrix} = \begin{bmatrix} \mathbf{q}_D \cdot \mathbf{v}_D & -\mathbf{q}_D \cdot \mathbf{v}_{I1} \\ \mathbf{q}_{I1} \cdot \mathbf{v}_D & -\mathbf{q}_{I1} \cdot \mathbf{v}_{I1} \end{bmatrix}^{-1} \begin{bmatrix} \mathbf{q}_D \cdot \mathbf{q}_{I1} - \|\mathbf{q}_D\|^2 \\ \|\mathbf{q}_{I1}\|^2 - \mathbf{q}_D \cdot \mathbf{q}_{I1} \end{bmatrix}$$

For the process described above, we use the following relations presented in Fig. 7. We use ray tracing [14] to describe the light paths to estimate the object distance. (1) Intersection of a ray from a point.

$$\mathbf{q}(\mathbf{p}, \mathbf{v}, \mathbf{s}, \hat{\mathbf{n}}) = \mathbf{p} + \mathbf{v}\frac{(\mathbf{s}-\mathbf{p}) \cdot \hat{\mathbf{n}}}{\mathbf{v} \cdot \hat{\mathbf{n}}} \tag{11}$$

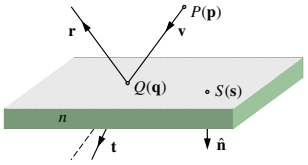

Figure 7. A ray and a normal vector of the plate.

(2) Reflection vector on a surface.

$$\mathbf{r}(\mathbf{v}, \hat{\mathbf{n}}) = \mathbf{v} - 2\hat{\mathbf{n}}\|\mathbf{v} \cdot \hat{\mathbf{n}}\| \tag{12}$$

(3) Refraction vector.

$$\mathbf{t}(\mathbf{v}, \hat{\mathbf{n}}, n) = k_f \left(\frac{\mathbf{v}}{\|\mathbf{v} \cdot \hat{\mathbf{n}}\|} - \hat{\mathbf{n}} \right) + \hat{\mathbf{n}} \tag{13}$$

$$k_f = \frac{1}{\sqrt{n^2 \left\| \frac{\mathbf{v}}{\|\mathbf{v} \cdot \hat{\mathbf{n}}\|} \right\|^2 - \left\| \frac{\mathbf{v}}{\|\mathbf{v} \cdot \hat{\mathbf{n}}\|} - \hat{\mathbf{n}} \right\|^2}}$$

3.3. Constraint in Reflection Stereo

The relative displacement $\mathbf{d}_p^*(\mathbf{a})$ of the rear-surface reflection image from the surface reflection image for an object at infinite distance and the unit vector $\mathbf{e}^*(\mathbf{a})$ of the constraint line for an image position $\mathbf{a}$ are obtainable from extrinsic parameters.

An object range along the lens optical axis (Z-axis) $\hat{\mathbf{p}}_{Oz}(\mathbf{a}, \mathbf{d}|\mathbf{p}_e(\mathbf{a}))$ is obtainable from extrinsic parameters $\mathbf{p}_e(\mathbf{a})$ and a relative displacement $\mathbf{d}$ in the complex image. Using this relation, the displacement $\mathbf{d}$ is obtainable for a known object distance $\mathbf{p}_{Oz}$ using a one-parameter optimization problem.

The displacement $\mathbf{d}_p^*(\mathbf{a})$ is a convergence vector obtained by increasing the known distance. The unit vector of the constraint line $\mathbf{e}^*(\mathbf{a})$ can be estimated from multiple displacements for known distances. Obtaining these constraint parameters in the transmission-type configuration is done in the same way.

4. Calibration

The extrinsic parameters can be estimated from M sets of the object distance D_z and its corresponding displacement $\mathbf{d}$ for position $\mathbf{a}$ in a complex image, as follows.

$$\hat{\mathbf{p}}_e(\mathbf{a}) = \arg\min_{\mathbf{p}_e(\mathbf{a})} E(\mathbf{a}) \tag{14}$$

$$E(\mathbf{a}) = \sum_{i=1}^{M} \|D_{zi} - \hat{\mathbf{p}}_{Oz}(\mathbf{a}, \mathbf{d}_i|\mathbf{p}_e(\mathbf{a}))\|^2 + \alpha \|\tilde{\mathbf{p}}_e - \mathbf{p}_e(\mathbf{a})\|^2$$

It is analogous to the calibration method for stereo vision [15]. The second term in the objective function $E(\mathbf{a})$ is a stabilization term that prevents the estimated parameters from deviating markedly from design (catalogue) values $\tilde{\mathbf{p}}_e$. The weight α is set empirically to the minimum value. We have used the conjugate gradient method to minimize the nonlinear objective function with initial parameters of the design values.

The displacement $\mathbf{d}$ in a complex image can be detected as the second peak location of the autocorrelation function of the complex image without any knowledge of the constraint if the image contains a rich and dense texture. The seven components in the extrinsic parameters can be estimated from $M \geq 4$ sets of observations.

The estimated parameters are considered as continuous and their changes are small with respect to the image position, as is clear from observations of real acrylic plates. The following parametric expression with a 2D cubic function with respect to the image position $\mathbf{a} = (u, v)$ is used for range estimation.

$$\bar{\mathbf{p}}_e(\mathbf{a}) = \Phi_1 + \Phi_2 u + \Phi_3 v + \Phi_4 uv + \Phi_5 u^2 + \Phi_6 v^2 + \Phi_7 u^2 v + \Phi_8 uv^2 + \Phi_9 u^3 + \Phi_{10} v^3 \tag{15}$$

In that expression, $\Phi_j (j = 1, 2, .., 10)$ denotes coefficient vectors corresponding to the seven components of the extrinsic parameters. These vectors are obtainable using least-squares estimation, with estimated extrinsic parameters $\hat{\mathbf{p}}_e(\mathbf{a}_l)$ at image positions $\mathbf{a}_l$, as follows.

$$\Phi_j = \arg\min_{\Phi_j} \sum_l \|\bar{\mathbf{p}}_e(\mathbf{a}_l) - \hat{\mathbf{p}}_e(\mathbf{a}_l)\|^2 \tag{16}$$

Fourier series expansion can also be used for the expression for the extrinsic parameters instead of the 2D cubic approximation. But, we can read directly from Eq. (15) the estimated typical plate thickness and refractive index of the plate in Φ_1 along with their first order derivation with respect to horizontal and vertical directions in Φ_2 and Φ_3. The third order coefficients take very small values; the residuals in Eq. (16) are sufficiently small.

The constraint line direction and the infinite object position with respect to the image position are also obtained in advance, as described in **3.3.**, and are parameterized similarly as the extrinsic parameters for range estimation.

The object range is directly obtainable with the displacement in the complex image and these total 10 parametric expressions with 10 coefficients in each expression for a given image position.

5. Rectification

The correspondence search in a rectified stereo image pair [1] is much faster than that in an untouched

image pair because of the elimination of image interpolation.

In the reflection stereo, the correspondence search is done along the constraint line in a single complex image for a point of interest. In real computation, a small region with its center on the interest point and the same size region with its center on the constraint line are compared to obtain the correspondence position. Image interpolation could be done more efficiently if the constraint line were parallel to v-axis in the complex image by an image transformation.

As shown in **3.3.**, the relative displacement $\mathbf{d}_p^*(\mathbf{a})$ for an object at infinite distance, and the unit vector $\mathbf{e}^*(\mathbf{a})$ of the constraint line for an image position $\mathbf{a}$ is obtainable from extrinsic parameters. The constraint line for arbitrary image position $\mathbf{a} = (u, v)$ can become parallel to v-axis using the displacement and vector as

$$\begin{cases} u_r = u + \displaystyle\int_C^v \left\{\mathbf{e}^*(\mathbf{d}_p^{*-1}(\mathbf{a}))\right\}_u dv \equiv u + R(\mathbf{a}) \\ v_r = v \end{cases}, \tag{17}$$

where $\mathbf{a}_r = (u_r, v_r)$ and $\mathbf{a} = (u, v)$ respectively denote the rectified and pre-rectified image positions. Furthermore, C is a constant, and $\mathbf{d}_p^{*-1}(\mathbf{a})$ is a function that returns $\mathbf{a}'$, satisfying $\mathbf{a}' + \mathbf{d}_p^*(\mathbf{a}') = \mathbf{a}$. Also, $\{\}_u$ represents the u component in a vector.

The transformation reduces or stretches the complex image horizontally, although no transformation is seen at line $v = C$. The constant C can be given to minimize the sum of transformation quantity $\sum_l |R(\mathbf{a}_l)|$ for many image positions. In the experiment, $C = 0$ is used because the sum will take a minimum value at around $C = 0$ in real situations.

The transformation, which includes an inverse function and a definite integral, can not be described analytically. The following parametric expression is obtainable, in the same manner as the extrinsic parameters, from computational results of Eq. (17) at many locations in the image.

$$\begin{aligned} R(\mathbf{a}) = r_1 + r_2 u + r_3 v + r_4 uv + r_5 u^2 + r_6 v^2 \\ + r_7 u^2 v + r_8 u v^2 + r_9 u^3 + r_{10} v^3 \end{aligned} \tag{18}$$

These coefficients $r_j (j = 1, 2, .., 10)$ are used as the rectification parameter. The parametric expression converts a position in the pre-rectified image to a position in the rectified image.

On the other hand, the inverse function of Eq. (17)

$$u = u_r - R'(\mathbf{a}_r) \tag{19}$$

converts the image position in the rectified image to a position in the pre-rectified image. The inverse function is indispensable to obtain the rectified image. It is an inverse function of a cubic function; the exact solution is obtainable using Cardano's solution to the cubic. However, Newton's method with an initial value of u_r gives a solution with sufficient precision after only a few iterations.

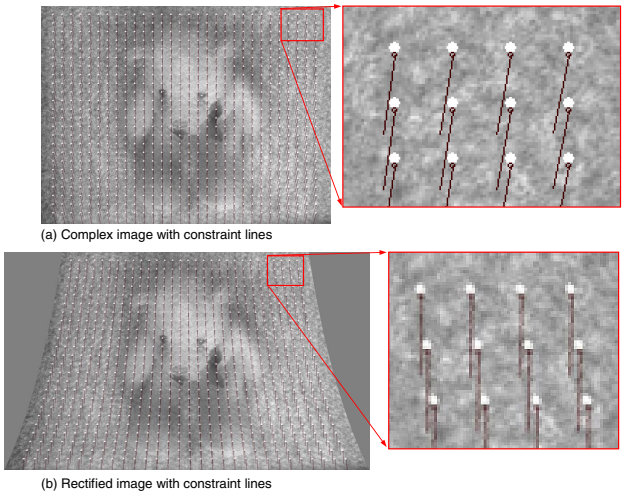

Figure 8. Complex image rectification.

Figure 8(a) portrays a complex image with constraint lines in many positions. The white circles represent the interest positions; the small black circles and lines respectively represent the relative displacement for an object at infinite distance and the constraint lines. Figure 8(b) shows an example of the rectified complex image. The constraint lines are transformed as parallel to the v-axis.

6. Experimental Results

The following experiments were conducted to demonstrate the effectiveness of the proposed calibration and rectification methods in the reflection stereo. The transmission-type configuration is used in **6.1.**, **6.2.** and **6.3.**; the reflection-type is used in **6.4.**.

6.1. Experimental Configuration

The experimental system was constructed as shown in Fig. 9. The double-sided half-mirror plate with a 75% reflection ratio is set with an angle $\pi/4$ for the optical axis. The system includes a black and white camera (60 FPS, IEEE1394, Flea; Point Gray Research Inc.). The design values of the plate are 12.0 [mm] thickness with a relative refraction index of 1.49. The measured distance from the lens optical center to the plate along the optical axis is $D_{co} = 66.2$ [mm]. We used a well-known camera calibration tool [2] for intrinsic parameter estimation. The calibrated parameters are the focal length $f/\delta = 1255.7$; the image size is

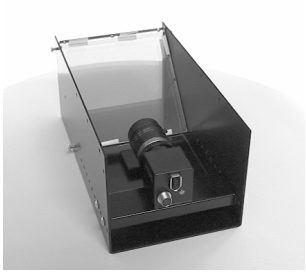

Figure 9. Configuration of the experimental system.

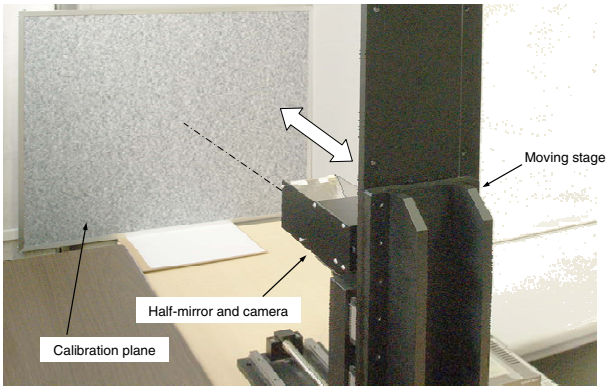

Figure 10. Setup of the calibration target.

640×480 [pixel]. Image distortion was alleviated using the estimated lens distortion parameters.

6.2. Calibration

As presented in Fig. 10, the experimental configuration is mounted on a one-directional moving stage. The stage moves accurately at a distance of 50 [mm] step to a frontal parallel target plane. The target plane has a rich texture to aid detection of the second and third peak in the autocorrelation function.

The displacements in the complex image are estimated at 24×18 $(= 432)$ positions. The region size is 35×35 [pixel]. In some image positions, the displacements are not obtained because of the loss or bias of the texture. The estimated displacements are compared with those of the neighbors to check their validity. The parametric expressions for the estimated 2D displacements are obtained using the valid displacements; then the extrinsic parameters are estimated using the parametric expressions.

The target positions are at $D_{zi} = 350 + 50i + D_e$ [mm] $(i = 1, 2, .., 13)$ from the optical center in Z-axis, where D_e is an unknown offset. To estimate D_e, first the following sum of the residuals with three predetermined values $(D_e = 0, \pm 25)$ is obtained; then the three sums of residuals are used to estimate the D_e for the minimum sum by a parabola fitted over the three

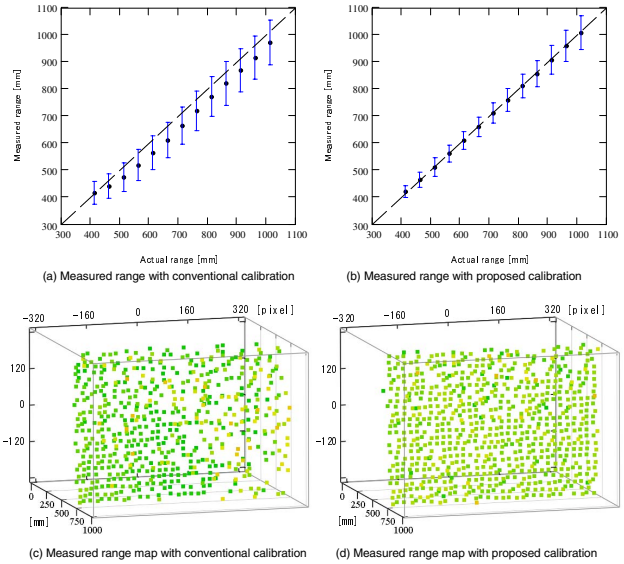

Figure 11. Range estimation results for the calibration plane at known distances.

sums.

$$\sum_{l} \sum_{i=1}^{13} \left\| (350 + 50i + D_e) - \hat{\mathbf{p}}_{Oz} \left(\mathbf{a}_l, \mathbf{d}_i | \mathbf{p}_e(\mathbf{a}_l) \right) \right\|^2$$

From the experiments, we have $D_e = 14.4662$ [mm].

6.3. Range to the Calibration Target

In these results, the target distance is measured again using the estimated calibration parameters.

Figures 11(a) and 11(b) respectively portray the range estimation linearity obtained using the conventional method [12] and the proposed method. The black circles and the range bars respectively represent the measured average and the standard deviation. The estimated range obtained using the conventional method has a bias error because uncalibrated system parameters are used, although no bias error is observed, as depicted in Fig. 11(b).

Figures 11(c) and 11(d) respectively show the estimated range maps obtained using the conventional and the proposed method. Inaccurate constraints used in the conventional method result in a widely varying range estimation. In contrast to this, the proposed calibration helps to detect the true displacement along the accurate constraint line in the complex image, resulting in a smooth estimation range.

6.4. Object Shape Measurement

The reflection-type configuration is used in this experiment. The design values of the plate are 12.0 [mm] thickness, the relative refraction index of 1.49, and the

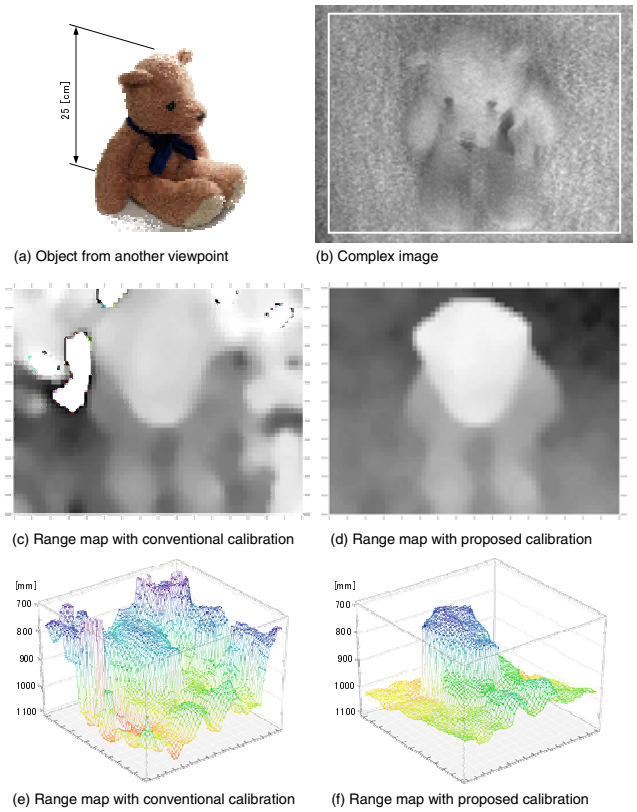

Figure 12. Object shape measurement results obtained using conventional and proposed calibration methods.

measured distance from the lens optical center to the plate along the optical axis of $D_{co} = 26.2$ [mm]. The intrinsic camera parameters are identical to those used in previous experiments.

Figure 12 shows the results. Figures 12(c) and 12(e) depict the measured range map obtained using the conventional method, whereas 12(d) and 12(f) depict the map obtained using the proposed method. Some background regions are missed in the conventional method, but the proposed method provides a stable and fine result.

7. Conclusions

This paper has presented an extrinsic parameter calibration and image rectification method for a reflection stereo using multiple planar targets with random texture at known distances. The calibrated extrinsic parameters represent the normal vectors of the plate surfaces, plate thickness, relative refraction index, and the plate position. Experimental results demonstrate the effectiveness of the proposed method.

Acknowledgement

This study was partially supported by Grant-in-Aid for Scientific Research (KAKENHI) (19300057).

References

[1] N. Ayache, and C. Hansen, "Rectification of Images for Binocular and Trinocular Stereo Vision," CVPR, pp. 11–16, 1988.

[2] J.-Y. Bouguet, "Camera Calibration Toolbox for Matlab," http://www.vision.caltech.edu/bouguetj/calib_doc/index.html, February 2007.

[3] C. Gao and N. Ahuja, "A Refractive Camera for Acquiring Stereo and Super-resolution Images," CVPR, pp. 2316–2323, 2006.

[4] J. M. Gluckman and S. K. Nayar, "Catadioptric Stereo using Planar Mirrors," IJCV, vol. 44, no. 1, pp. 65–79, 2001.

[5] S. Hiura and T. Matsuyama, "Depth Measurement by the Multi-Focus Camera," CVPR, pp. 953–959, 1998.

[6] K. N. Kutulakos and E. Steger, "A Theory of Refractive and Specular 3D Shape by Light-Path Triangulation," ICCV, vol. 2, pp. 1448–1455, 2005.

[7] D.-H. Lee and I.-S. Kweon, "A Novel Stereo Camera System by a Biprism," IEEE Trans. on Robotics and Automation, vol. 16, no. 5, pp. 528–541, 2000.

[8] Y. Manabe, M. Tsujita, and K. Chihara, "Measurement of Shape and Refractive Index of Transparent Object," ICPR, vol. 2, pp. 23–26, 2004.

[9] H. Murase, "Surface Shape Reconstruction of a Nonrigid Transport Object using Refraction and Motion," IEEE Trans. on PAMI, vol. 14, no. 10, pp. 1045–1052, 1992.

[10] Y. Nishimoto and Y. Shirai, "A Feature-Based Stereo Model using Small Disparities," Proc. on IEEE International Workshop on Industrial Applications of Machine Vision and Machine Intelligence, Seiken Symposium, pp. 192–196, 1987.

[11] T. P. Pachidis and J. N. Lygouras, "Pseudo-Stereo Vision System: A Detailed Study," Journal of Intelligent and Robotic Systems, vol. 42, no. 2, pp. 135–167, 2005.

[12] M. Shimizu and M. Okutomi, "Reflection Stereo – Novel Monocular Stereo using a Transparent Plate –," Proc. on Canadian Conference on Computer and Robot Vision, p. 14 (CD-ROM), 2006.

[13] M. Shimizu and M. Okutomi, "Monocular Range Estimation through a Double-Sided Half-Mirror Plate," Proc. on Canadian Conference on Computer and Robot Vision, pp. 347–354, 2007.

[14] T. Whitted, "An Improved Illumination Model for Shaded Display," Communications of the ACM, vol. 23, no. 6, pp. 343–349, 1980.

[15] Z. Zhang, "Flexible Camera Calibration by Viewing a Plane from Unknown Orientations," ICCV, vol, 1, pp. 666–673, 1999.